Machine Vision and Applications (2003) 15: 76–91
Digital Object Identifier (DOI) 10.1007/s00138-003-0131-4

Machine Vision and Applications

A CAD-based 3D data acquisition strategy for inspection

Flavio Prieto[1], **Richard Lepage**[2], **Pierre Boulanger**[3], **Tanneguy Redarce**[4]

[1] Universidad Nacional de Colombia Sede Manizales, Grupo de Percepción y Control Inteligente, Carrera 27 # 64–60, Manizales (Caldas), Colombia
[2] École de Technologie Supérieure, Laboratoire d'Imagerie, de Vision et d'Intelligence Artificielle, 1100 rue Notre-Dame Ouest, Montréal, Québec, H3C 1K3, Canada
[3] University of Alberta, Department of Computing Science, 2–21 Athabasca Hall, Edmonton, Alberta, T6G 2E8, Canada
[4] Institut National des Sciences Appliquées de Lyon, Laboratoire d'Automatique Industrielle, 20 avenue Albert Einstein, 69621 Villeurbanne Cedex, France

Received: 6 May 2001 / Accepted: 8 November 2002
Published online: 13 November 2003 –

Abstract. The use of a laser range sensor in the 3D digitalization process allows significant improvement in acquisition speed and in 3D measurement point density. However, if we want to use these 3D data in applications that require data with a high degree of accuracy like inspection tasks, it is mandatory that the 3D points be acquired under the best conditions of accuracy. During 3D capture of a part, several sources of error can alter the measured values. Thus we must find and model the most important parameters affecting the accuracy of the range sensor. This error model, along with the CAD model of the part, is used to produce a sensing plan to completely and accurately acquire the geometry of the part. The sensing plan is comprised of the set of viewpoints that defines the exact position and orientation of the camera relative to the part. There is no limitation with regard to the shape of the part to be digitalized. An autosynchronized range sensor fixed on a coordinate measuring machine was used. For this sensor, the accuracy of the 3D measured points is a function of the distance and of the angle of incidence relative to the surface. The strategy proposed to find the acquisition plan guarantees that the viewpoints meet the best accuracy conditions in the scanning process, solving the occlusion problems. It was found that the 3D data acquired by using the proposed strategy are around 30% more accurate than the 3D data obtained in a standard acquisition.

Key words: View planning – Range sensor – Range image – Inspection – CAD-based vision

1 Introduction

Automatic inspection using range sensors is a complex task that requires an exact geometrical definition of the part and a large number of measurement points. The use of a coordinate measuring machine (CMM) as a positioning device and recent progress in laser sensors combining measurement accuracy and fast acquisition speed allow one to obtain more accurate 3D measurements. These 3D points represent an explicit description of object surfaces. In addition, knowledge of the corresponding CAD model provides an exact and complete description of the geometry of the object under inspection. We have developed a method for automatic inspection of parts containing curved surfaces [11]. The system uses a CAD model (in IGES format) and 3D data provided by a range sensor fixed to a CMM. The quality of the results depends almost exclusively on the accuracy of measurements.

At present, it is nearly impossible to compare the accuracy obtained with a CMM equipped with a contact sensor (lower than a micron) and those delivered by a CMM equipped with a laser range finder (about 25 μm at best). But the inspection task with the contact sensor is too slow compared to the range sensor. In addition, in the inspection process of soft parts, the contact sensor could affect the part. If one wants to take advantage of the increase in the speed of acquisition obtained with a range sensor to make a systematic dimensional check of manufactured parts, it is necessary to attain the best possible accuracy of the depth images obtained with a range sensor.

In this paper, we present a 3D data acquisition strategy to improve the overall accuracy of the data obtained with a range sensor fixed to a CMM. The strategy uses the CAD model of the part and the error model of the range sensor to select the best sensor placement in the digitalization process. The high-accuracy 3D data obtained would be very useful for inspection tasks. In addition, in inspection we are often interested in checking the tolerances of just some surfaces. This strategy allows one to digitalize the surfaces of interest or the whole part. Due to the mechanical support where the laser sensor is fixed, we only give results for the inspection of small objects. Occlusion problems are solved in such a way that the acquired 3D data remain as accurate as possible.

A review of previous work on sensor planning for inspection is presented in Sect. 2. In Sect. 3, we present an experimental setup to determine and evaluate the parameters that influence the accuracy of the 3D data obtained from the range sensor. With this experiment we find a model of the 3D data

Correspondence to: F. Prieto
(e-mail: fprieto@nevado.manizales.unal.edu.co)

accuracy as a function of those parameters. The problem of the range sensor placement is posed in Sect. 4. In Sect. 5, we present an acquisition planning strategy for a digitalization system built from an autosynchronized range sensor fixed on a CMM in order to improve the 3D data accuracy. Finally, in Sect. 6, we show the improvement of accuracy when such a strategy is used.

2 Literature review

Three-dimensional range sensor planning is a complex task. The problem can be stated as follows. Given the information related to the environment (object under observation, available sensor) and the task the measurement system must achieve (feature detection, recognition, inspection), design strategies automatically determine the parameters of the sensors (optics, position, and orientation) in order to carry out the measurement task within a specified precision range.

Tarabanis et al. [14] provide an interesting survey of sensor planning strategies based on model-based vision algorithms (e.g., camera, range sensor, illumination systems). The survey is divided into three main topics: (1) the detection of an object's features, (2) model-based digitalization strategies for recognition and location, and (3) the reconstruction problem.

The definition and implementation of the planning algorithm are related to measurement goals and available tools. When the goal of the 3D measurements is toward the detection and inspection of an object's features [1,4,15–19], an accurate model of the object must be found in order to fulfill the task. The model controls the offline digitalization process. In general, the digitalization strategy is optimized to acquire the whole object or the interesting features with a minimum number of viewpoints.

The design of the planning algorithm depends upon the type and number of sensors and upon the type of mechanical support. Sensors include range sensor [8,10,21], CCD camera [15], CCD camera coupled to a light source [5,17], or a set of CCD cameras [4,19]. Mechanical supports range from robot arms [15,21], robotized systems [20], translation table [4,5,8,19], or rotation table [10,17]. In the literature, we did not find any work with a CMM as the mechanical support in the way we used it in our work.

According to the goals of the digitalization system, every acquisition strategy must adapt to the system constraints (topology and size of object to be digitalized, object model, etc.). The output of the algorithm is the whole set of viewpoints for the digitalization (position, orientation, and sensor trajectory). The viewpoint parameters are obtained by optimizing the number of viewpoints, the amount of data acquired, minimal trajectory, etc. The parameters must also obey system constraints like object visibility and a sensor trajectory free of collisions.

In this paper, we define and implement an algorithm for 3D acquisition using a high-precision sensor mounted on a CMM. The main goal to be attained with this algorithm is to provide accurate real-time 3D data for tolerance control of industrial parts by improving the accuracy of the acquired data.

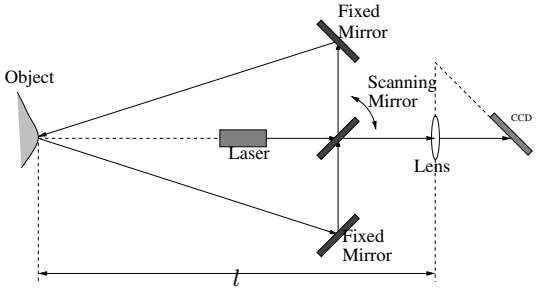

Fig. 1. Optical setup of the NRCC synchronized range sensor

3 The 3D range camera

This section describes the optical principle of the range camera used and the accuracy of the 3D data acquired as a function of the camera placement. The camera, an autosynchronized range (ASR) sensor, was developed at the National Research Council of Canada [3,13].

3.1 Optical principle

The basic geometry of this 3D laser camera is based on the synchronization of the projected laser beam with its return path. The main advantage of this approach is that it allows one to simultaneously obtain high resolution and a large field of view, as opposed to standard triangulation geometries where a compromise is made between resolution and field of view. The synchronized scanning geometry is based on a double-sided mirror used to project and detect a focused or collimated laser beam (Fig. 1). The rotation of this mirror defines the sweep of the laser beam (called angle γ in Sect. 4).

The scanning of the target surface by the sensor results in the output of 3D points (x, y, z) and their luminous intensity (I) at the surface. The ASR sensor explores a surface line by line at a density that can be specified by the user (usually 512 points per line). The depth (z coordinate) is measured for every x coordinate provided by the mirror position. In order to scan the whole part and to allow precise mechanical registration between views, the range sensor must be fixed on a mechanical support. For our experimental setup, the ASR sensor is mounted on a coordinate measuring machine. The CMM movement provides the y coordinate. The CMM allows six degrees of freedom, three for the space position and three for the orientation of the sensor. The acquisition system (mechanical support and ASR sensor) limits the workspace, that is, the space where the part to be digitalized must be enclosed. For our system, this space is a parallelepiped where the sides ws_x, ws_y, and ws_z represent, respectively, maximum displacements of the sensor in the directions x, y, and z in such a way that the sensor is always oriented toward the center of the workspace. The dimensions of the workspace are $ws_x = 80\,\text{cm}$, $ws_y = 30\,\text{cm}$, and $ws_z = 30\,\text{cm}$.

3.2 Noise model of the digitalization system

In order to model the noise, we are generally interested in obtaining a characterization of the noise introduced at each 3D measurement point. This characterization is related to a

certain number of parameters such as the distance from the sensor to the surface and the incidence angle between the laser beam, when it reaches the surface, and the normal vector to the part. The latter one affects primarily the sensor position. If we suppose that the noise in an image is additive and random, i.e., a random signal $b(x, z)$ is added to the real values of the image (x, z), then $(\hat{x}, \hat{z}) = (x, z) + b(x, z)$. The quantity of noise in an image is estimated by the covariance matrix $\boldsymbol{\Sigma}$. Most of the time, the noise is modelled like a random function with a Gaussian distribution of zero mean value:

$$b(\vec{r}) = \frac{1}{(2\pi)^{3/2}\sqrt{|\boldsymbol{\Sigma}|}} exp\left(-\frac{1}{2}(\vec{r}-\vec{s})^T \boldsymbol{\Sigma}^{-1}(\vec{r}-\vec{s})\right) \quad (1)$$

where $\vec{s}$ is a 2D vector corresponding to the point on the surface of the given geometrical model nearest to $\vec{r}$, and $\boldsymbol{\Sigma}(\vec{r})$ is the covariance matrix for the measured point $\vec{r}$. The covariance matrix in Eq. 2 defines for the point $\vec{r}$ an ellipse whose form (length of axes) is a function of the distance from the sensor to the surface and of the incidence angle of the laser beam on the surface.

$$\boldsymbol{\Sigma} = \begin{pmatrix} \sigma_{xx} & \sigma_{xz} \\ \sigma_{zx} & \sigma_{zz} \end{pmatrix} \quad (2)$$

The components of the covariance matrix $\boldsymbol{\Sigma}$ are:

- σ_{xx}, variance in x
- σ_{xz} (σ_{zx}), covariance between x (z) and z (x)
- σ_{zz}, variance in z

In the first experiment, we averaged 256 measurements of the same 3D point. We found that the average value converges toward a constant mean value within 64 measurements. Therefore, we took 128 measurements to compute the variance at each point. In order to evaluate the accuracy of the cloud of 3D points obtained by the scanning process, we achieved 128 measurements in different positions for distance and orientation of the laser sensor with respect to a reference surface. The measurements were completed after the camera calibration process and camera placements approached the calibration conditions.

The objective of those measurements is to determine the covariance matrix Σ, which we define as the addition of the covariance introduced by each incident angle and by the object-sensor distance. From the experiments it can be seen that these criteria are independent. Thus the covariance matrix is defined by:

$$\boldsymbol{\Sigma} = \boldsymbol{\Sigma}(\alpha) + \boldsymbol{\Sigma}(\beta) + \boldsymbol{\Sigma}(d) \quad (3)$$

where:

- α is the angle of incidence of the laser beam on the surface in the direction of the laser sweep [defined around the y-axis in Fig. 2(a)]. In the figure, the ASR sensor is seen from the side (perpendicular to the xz plane), the dotted lines represent the limits of the laser sweeping beam (done by moving along the x-axis).
- β is the angle of incidence of the laser beam on the surface in the perpendicular direction to the laser sweep [defined around the x-axis in Fig. 2(b)]. In the figure, the ASR sensor is seen from the top (perpendicular to the plan yz), the sweeping of the laser beam is done by moving along the x-axis (aligned with the projection of the laser beam represented by the continuous line from the sensor to the surface).
- d is the distance from the range sensor to the surface.

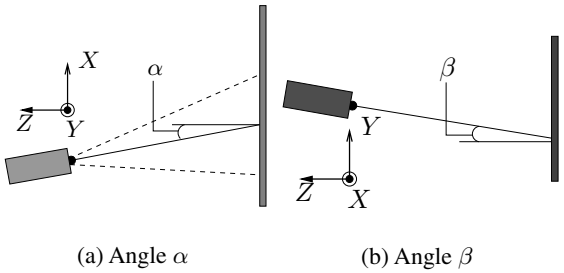

(a) Angle α (b) Angle β

Fig. 2. Definition of the incident angles α and β

Contribution of α to the covariance matrix. To determine the components of the covariance matrix according to the angle of incidence α grouped in the matrix

$$\boldsymbol{\Sigma}(\alpha) = \begin{pmatrix} \sigma_{xx}(\alpha) & \sigma_{xz}(\alpha) \\ \sigma_{zx}(\alpha) & \sigma_{zz}(\alpha) \end{pmatrix}$$

we have varied the orientation angle of the range sensor in the direction of the laser beam sweep. The angle β and the distance d were fixed to the values $\beta = 0°$ and $d = 200\,\text{mm}$.

We show in Fig. 3 the shape of the variance σ_{xx} in x. In this figure and thereafter, the solid curve represents actual measurements and the dotted curve is for the best fit approximation. Although the approximation appears a little coarse, it is the best approximation of the behavior of the real curve in the interval that will be specified for each curve. The scale of the y-axis is usually about $10^{-6}\,\text{mm}^2$.

The curve that best approximates the real values in the interval from $0°$ to $35°$ is defined by the equation:

$$\sigma_{xx}(\alpha) = 1.42 \times 10^{-7} \cdot e^{5.46\times10^{-2}\cdot|\alpha|} \quad (5)$$

Figure 4 shows the behavior of covariance σ_{xz}. The curve that best fits the measured values is given by:

$$\sigma_{xz}(\alpha) = \sigma_{zx}(\alpha) = 6.47 \times 10^{-7} \cdot e^{5.91\times10^{-2}\cdot|\alpha|} \quad (6)$$

Finally, we show in Fig. 5 the behavior of the variance in z (σ_{zz}). The next equation defines the curve that best fits the real values.

$$\sigma_{zz}(\alpha) = 3.77 \times 10^{-6} \cdot e^{6.01\times10^{-2}\cdot|\alpha|} \quad (7)$$

The behavior of the components of the covariance matrix is exponential. Therefore, a smaller value of dispersion is produced for an incident angle near zero degrees, which suggests an optimal placement for the sensor in the normal direction on the surface. The fitting curve displays sufficiently constant and low values in the interval $0° \leq \alpha \leq 35°$. The incident angle of the laser beam should be restricted to the range $-35° \leq \alpha \leq 35°$ at measurement time.

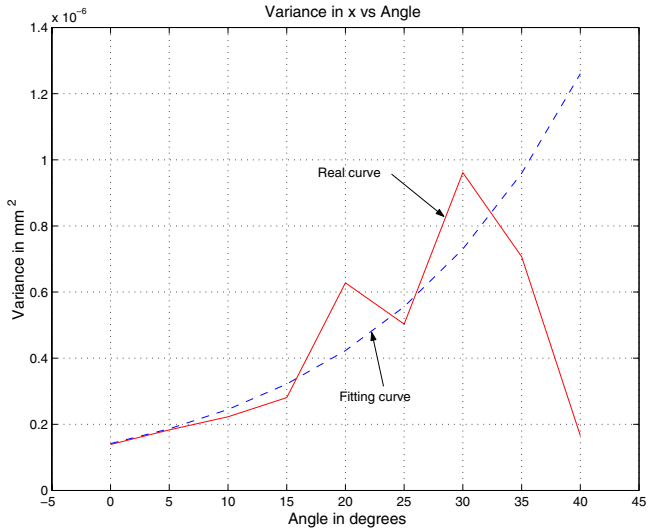

Fig. 3. Variance in x vs. the incident angle α

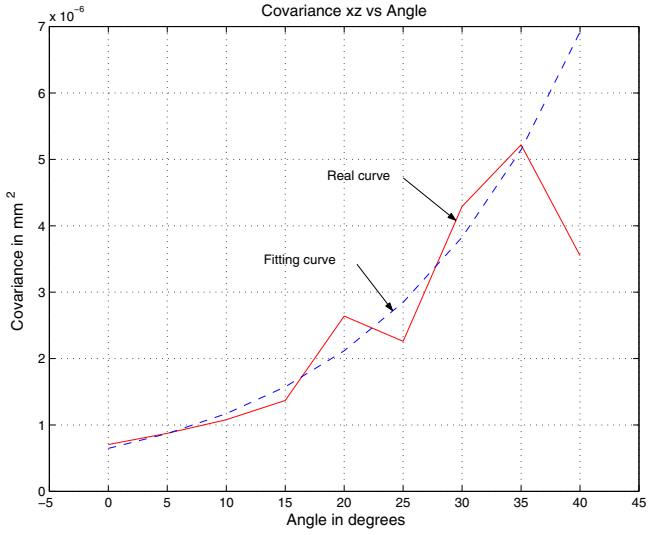

Fig. 4. Covariance xz vs. the incident angle α

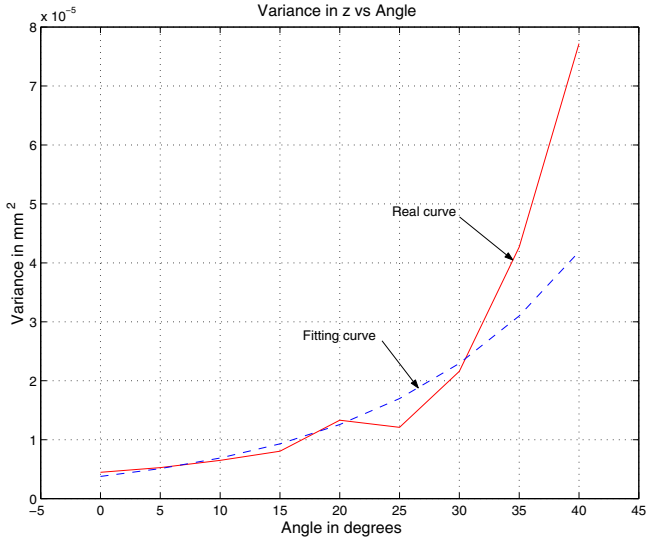

Fig. 5. Variance in z vs. the incident angle α

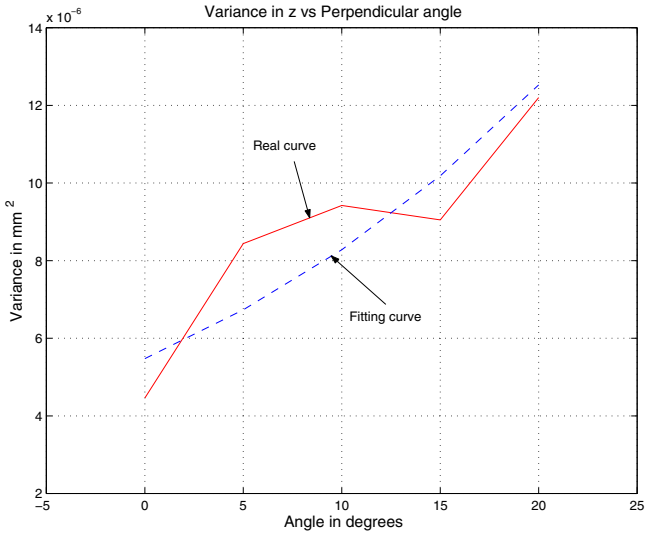

Fig. 6. Variance in z vs. the incident angle β

In Figs. 3, 4, and 5, we observe $\sigma_{zz} > \sigma_{xz} > \sigma_{xx}$. The variance in the z direction is at least ten times larger than the variance in the x direction.

Contribution of β to the covariance matrix. The covariance matrix according to the incident angle β, $\Sigma(\beta)$ was determined by changing the orientation of the range sensor in a perpendicular direction from that of the laser beam sweep. In this case, the angle α and the distance d were fixed to: $\alpha = 0°$ and $d = 200\,\text{mm}$.

Figure 6 shows the behavior of the variance in z according to the incident angle β, $\sigma_{zz}(\beta)$. We do not present the curves σ_{xx} and σ_{xz} because they have the same behavior and are smaller in amplitude. The curve that best fits the real curve is the exponential curve defined by Eq. 10. Equations 8 and 9 define the behavior of the variance σ_{xx} in x and the covariance σ_{xz} in xz.

$$\sigma_{xx}(\beta) = 1.59 \times 10^{-7} \cdot e^{4.59\times10^{-2}\cdot|\beta|} \tag{8}$$

$$\sigma_{xz}(\beta) = \sigma_{zx}(\beta) = 8.30 \times 10^{-7} \cdot e^{4.40\times10^{-2}\cdot|\beta|} \tag{9}$$

$$\sigma_{zz}(\beta) = 5.47 \times 10^{-6} \cdot e^{4.15\times10^{-2}\cdot|\beta|} \tag{10}$$

At the time of digitalization, the incident angle β should be restricted to the interval $-15° \leq \beta \leq 15°$.

Contribution of d to the covariance matrix. By changing the distance from the sensor to the surface, we have determined the covariance matrix for parameter d.

Figure 7 shows the behavior of the variance in z vs. the digitalization distance d, so $\sigma_{zz}(d)$. Here the angles α and β were fixed to $0°$.

Equations 11, 12, and 13 are the curves that best fit the real values of the variance in x, the covariance xz, and the variance in z, that is, σ_{xx}, σ_{xz}, and σ_{zz}, respectively.

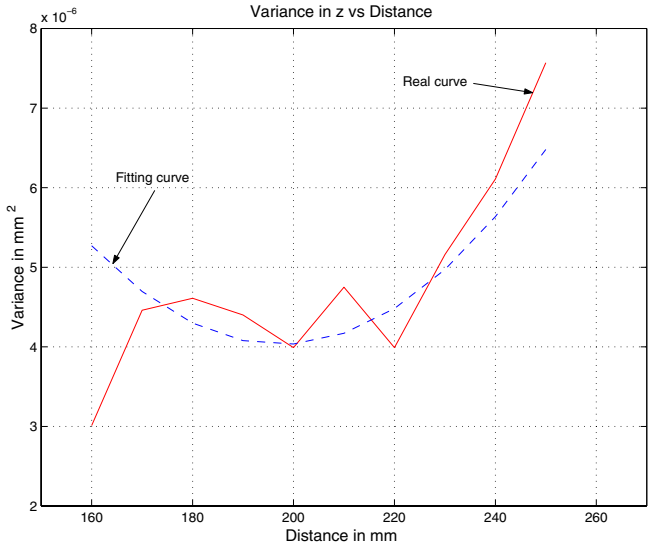

Fig. 7. Variance in z vs. the distance d

$$\sigma_{xx}(d) = 1.14 \times 10^{-11} \cdot d^2 - 4.20 \times 10^{-9} \cdot d + 5.20 \times 10^{-7} \quad (11)$$

$$\sigma_{xz}(d) = \sigma_{zx}(d) = 9.92 \times 10^{-11} \cdot d^2 - 3.82 \times 10^{-8} \cdot d + 4.34 \times 10^{-6} \quad (12)$$

$$\sigma_{zz}(d) = 8.86 \times 10^{-10} \cdot d^2 - 3.47 \times 10^{-7} \cdot d + 3.81 \times 10^{-5} \quad (13)$$

We conclude that at digitalization time the range sensor should be placed in the interval of distance $170\,\text{mm} \leq d \leq 240\,\text{mm}$.

These results confirm that we can improve the accuracy of the data acquisition process by following some criteria defined previously (normal direction, distance). Thus in order to be able to achieve inspection tasks, we have implemented an acquisition planning strategy. The strategy improves the 3D data accuracy by finding the best camera placement to digitalize a part, using the range of parameters α, β, and d computed in this section.

4 The range sensor placement problem

The main goal of this work is to improve the 3D data accuracy with the aid of a sensor placement strategy. Such a strategy consists in computing a set X of viewpoints x^i in order to obtain a complete and accurate 3D image of a surface or of the whole part. We define an accurate 3D image as a cloud of 3D points acquired by the scanning process in the best accuracy conditions. Our strategy is to find the collection of viewpoints for each surface independently. If one wants to digitalize the whole part, one has simply to add the assembly X of all the surfaces in the part.

We define a viewpoint as a set of seven parameters $x^i = \{x, y, z, \theta, \phi, \psi, \gamma\}^i$. Six parameters are from the mechanical support (CMM): three position parameters (x, y, z) and three orientation parameters (θ, ϕ, ψ). One parameter is from the ASR sensor specifying the instantaneous angle of the sweep (angle γ).

- *The position parameters.* These parameters in R^3 define the spatial placement of the camera relative to the coordinate system of the part. They are the coordinates (x, y, z).
- *The orientation parameters.* These parameters in R^3 define the direction that the ASR sensor must take at digitalization time. They are the Euler angles so (θ, ϕ, ψ). The angle θ defines the rotation around the z-axis, the angle ϕ defines the rotation around the y-axis, and the angle ψ defines the rotation around the x-axis.
- *A sweeping parameter.* The parameter γ specifies the instantaneous angle of the laser beam.

Figure 8 shows a viewpoint with all its parameters. These parameters can change and others can be added according to the type of range sensor and mechanical support used. We do not consider optical parameters, such as the focal distance and the opening of the lens, because we assume the system (range sensor plus mechanical support) has been previously calibrated. At the top of Fig. 8, ϕ and ψ depict the direction for measurement and not their magnitude, their actual value being, in fact, zero.

The set X of viewpoints x^i is defined by: $X = \{x^1 x^2 \dots x^i \dots x^n\}$, with n the minimum number of viewpoints to digitalize a simple surface or the whole part. A whole range image is obtained by moving the sensor throughout all the points of view in the set X. The ASR sensor movement between two consecutive viewpoints is performed following a straight line.

4.1 Constraints imposed on the acquisition strategy

The constraints imposed on our system, knowing that our interest is to have 3D data with a high degree of accuracy, are the following: size of the part, knowledge of the initial position and orientation of the part, and availability of the CAD model (in IGES format) of the part.

Size of the part. The only geometrical constraint imposed on the system lies in the dimensions of the part. The laser sensor, in order to sweep a given surface, must be fixed to a precisely drivable mechanical support. As stated in Sect. 3, we use a CMM as a mechanical support whose workspace is defined by $wk_x = 80\,\text{cm}$, $wk_y = 30\,\text{cm}$, and $wk_z = 30\,\text{cm}$. Thus the part to be inspected must be located inside the CMM workspace. The dimensions of all of the parts used in this work are included in a volume of $100 \times 50 \times 50\,\text{mm}$.

Position and orientation of the part. Knowledge of the position and orientation of the part enables one to register the reference system of the part with that of the laser sensor mechanical support. To deal with this constraint, we use a registration algorithm to register the 3D point cloud and the CAD model of the part, which was implemented by Moron [6,7] and is based on the well-known work of Besl and McKay [2]. If the part or the CAD model of the part is wrong, the registration process produces a large error between the model and the part. In this case, the acquisition strategy is stopped.

CAD Model. The system uses the CAD model of the part, in IGES format, not only in the process of registration but

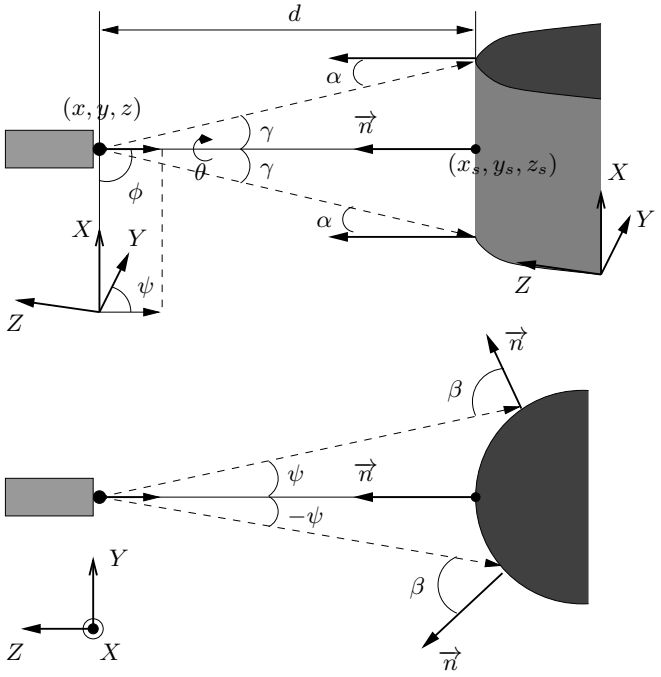

Fig. 8. Viewpoint parameters

also for searching the set X of digitalization viewpoints. The IGES format contains the exact representation of the part by using nonuniform rational B-spline (NURBS) surfaces. These surfaces are used for the computation of the sensor positions in space and as well as for the construction of a *voxel* model of the part (Sect. 5.2) to solve collision and occlusion problems.

4.2 Criteria for the acquisition strategy

We will now describe some criteria taken into account by the acquisition planning algorithm in order to produce a correct solution.

Position and orientation of the sensor at digitalization time. We saw in the previous section that the accuracy of the 3D data is a direct function of the conditions of digitalization such as the position and orientation of the camera. For this work, digitalization under the best conditions of accuracy is desirable. A first criterion to be respected is that the position and orientation parameters from each viewpoint must be in the best condition with respect to the accuracy of the data. In Sect. 5.2, we relate the parameters of a viewpoint to parameters α, β, and d and select the value of those parameters in order to improve the accuracy of the 3D data.

Visibility of surfaces to digitalize. The algorithm must guarantee that the area to be digitalized will be completely visible, i.e., the surface is not occluded. A surface is occluded for a specific viewpoint if any object intersects the laser beam before reaching the target surface or the reflected ray before it arrives at the reception device. An algorithm to evaluate the visibility must be implemented.

Data accuracy. To solve the visibility problem of certain surfaces, the sensor must be placed far away from the optimum conditions for digitalization; in this way a poor accuracy will be obtained. The system must evaluate the new accuracy of the 3D data and guarantee that it is better than the minimal accuracy required by the system.

Uniform distribution of the 3D points. The points obtained by the digitalization process must be distributed uniformly on the surfaces of the part. Moreover, the system must know the areas of the part that were already digitalized.

Set X of viewpoints distribution. The set X of viewpoints must be distributed to have minimal mechanical support displacements without collisions. The ASR sensor displacement between two viewpoints is made following a straight line. An algorithm to evaluate the collision problems during this displacement must be implemented. Although the objective of this acquisition strategy is not to minimize the number of viewpoints, it can be reduced when they are aligned, moving the sensor from the initial to the final point, as long as it is guaranteed there are no collision problems. To avoid collision during the CMM motion, a simple process that verifies that the CMM/sensor volume model does not intersect the volume of the inspected object during the motion was used.

5 The 3D data acquisition strategy

5.1 The optimization problem

In Sect. 3, we exposed the noise model of the digitalization system. Let $\vec{r}_{ij}$ be the value without noise of the point (x_i, z_j), and let $(\hat{x}_i, \hat{z}_j)$ be the measured value of the point. The noise model for a data point measured by the sensor is $(\hat{x}_i, \hat{z}_j) = (x_i, z_j) + b(x_i, z_j)$. The noise was described in Eq. 1 (and rewritten here) as a probability density function with a Gaussian distribution.

$$b(\vec{r}) = \frac{1}{(2\pi)^{3/2}\sqrt{|\boldsymbol{\Sigma}|}} exp\left(-\frac{1}{2}(\vec{r}-\vec{s})^T \boldsymbol{\Sigma}^{-1}(\vec{r}-\vec{s})\right) \quad (14)$$

The properties of the noise function $b(\vec{r})$ can be interpreted geometrically, assigning a constant probability value to the intersection of the function $b(\vec{r})$ with a horizontal plane. These intersections form a family of ellipses. When the center of the ellipse coincides with the origin of the reference frame, the form and the orientation are defined completely by Σ. Indeed, the length of the major and minor axes can be calculated easily as the square root of the eigenvalues of Σ. The length of the axes of the dispersion ellipse for the point $\vec{r}$ can then be calculated:

$$L_x(\vec{r}) = \sqrt{\frac{1}{2}(\sigma_{xx}(\vec{r}) + \sigma_{xz}(\vec{r}))}$$
$$L_z(\vec{r}) = \sqrt{\frac{1}{2}(\sigma_{xz}(\vec{r}) + \sigma_{zz}(\vec{r}))} \quad (15)$$

where $L_x(\vec{r})$ is the length of the minor axis and $L_z(\vec{r})$ is the length of the major axis, since for the point $\vec{r}$ we know that $\sigma_{zz}(\vec{r}) > \sigma_{xz}(\vec{r})$ (Sect. 3).

Thus, to obtain optimal 3D data with respect to the accuracy of the measurement system, we must minimize L_z with

respect to the dependent parameters α, β, and d. We solve as a minimization problem as follows:

$$\begin{aligned} minimize: \quad & \sigma_{xz}(\alpha) + \sigma_{xz}(\beta) + \sigma_{xz}(d) \\ & + \sigma_{zz}(\alpha) + \sigma_{zz}(\beta) + \sigma_{zz}(d) \\ subject\ to: \quad & |\alpha| \leq 35^\circ \\ & |\beta| \leq 15^\circ \\ & 170\,\text{mm} \leq d \leq 240\,\text{mm} \end{aligned} \tag{16}$$

The constraints for the minimization problem were obtained in Sect. 3. In this same section, we found the values for $\sigma_{xz}(\alpha), \sigma_{xz}(\beta), \sigma_{xz}(d), \sigma_{zz}(\alpha), \sigma_{zz}(\beta), \sigma_{zz}(d)$ (see Eqs.6, 9, 12, 7, 10, and 13, respectively).

The solution to this minimization problem through a gradient descent method, was $\alpha = 0^\circ, \beta = 0^\circ$, and $d = 195$ mm. Those values correspond to the case where the laser beam, when the sweeping angle is equal to zero ($\gamma = 0^\circ$), reaches the surface perpendicularly ($\alpha = 0^\circ, \beta = 0^\circ$) and the ASR sensor is located at a distance (d) of 195 mm. This position is in general attainable by the sensor when external surfaces of the part are being digitalized (surfaces free of occlusion). For the digitalization of an internal surface, the system will detect the existence of an occlusion problem and will automatically look for a new viewpoint. This process will be described in the following subsections.

5.2 The implemented acquisition strategy

Now that we have posed the optimization problem, we describe a pseudocode describing our algorithm implemented as a solution to the acquisition strategy problem.

3D data acquisition strategy algorithm
1. *Input data.*
   - 1.1. *Extract data from the CAD model.*
   - 1.2. *Generate the 3D voxel model.*
2. *Find the viewpoint set.*
   - 2.1. *Viewpoint projection on the surface.*
   - 2.2. *Find the best viewpoint placement.*
   - 2.3. *Verify the nonocclusion conditions.*
3. *Estimate 3D data accuracy.*
4. *Distribute the set X of viewpoints.*

In the following paragraphs, we will describe each step of this algorithm.

5.2.1 Step 1: Input data

Two processes generate the input data required for the algorithm. A first process extracts from the CAD file the needed data to search for viewpoints on the surfaces. The second process generates a 3D voxel model of the part.

Step 1.1: Extract data from the CAD model. A CAD model of the part in IGES format is input to the algorithm. The IGES file contains the exact representation of the part by using NURBS surface parameters. A NURBS surface of order p in the parametric direction u and of order q in the parametric direction v is defined by the following equation:

$$\vec{s}(u,v) = \frac{\sum_{i=0}^{n}\sum_{j=0}^{m} N_{i,p}(u) N_{j,q}(v) w_{i,j} \vec{P}_{i,j}}{\sum_{i=0}^{n}\sum_{j=0}^{m} N_{i,p}(u) N_{j,q}(v) w_{i,j}} \tag{17}$$

with n and m being the number of control points in the parametric direction u and v, respectively, $\vec{P}_{i,j}$ the control points, $w_{i,j}$ the weight associated with the control point $\vec{P}_{i,j}$, and $N_{i,p}$ (or $N_{j,q}$) the B-spline base functions defined by the following recurrent formula:

$N_{i,p}(u) = \frac{u-u_{i-1}}{u_{i+p-1}-u_{i-1}} N_{i,p-1}(u) + \frac{u_{i+p}-u}{u_{i+p}-u_i} N_{i+1,p-1}(u)$ and

$$N_{i,0}(u) = \begin{cases} 1 \text{ if } u_{i-1} \leq u \leq u_i \\ 0 \text{ elsewhere} \end{cases},$$

where u_i, v_j are the inner knots belonging to the knot vectors of the NURBS surface, $u_i \in [u_0, u_1]$ and $v_j \in [v_0, v_1]$. The range of variations for parameters u and v is defined by $u_0 \leq u \leq u_1$ and $v_0 \leq v \leq v_1$. That means that all values of u and v must be within the interval $[u_0, u_1]$ and $[v_0, v_1]$, where u_0, u_1, v_0, and v_1 are the extremes of the parametric surface. For more details about NURBS, refer to [9].

Step 1.2: Generate the 3D voxel model. Let T be a linear transformation that transforms a point (u, v) in the parametric space toward a point (x, y, z) in the 3D space, so that $T(f(u,v)) = (X(f(u,v)), Y(f(u,v)), Z(f(u,v)))$. Let $P(u, v)$ be a 3D surface representation of a part defined by the union of its N parametric surfaces

$$P(u,v) = \sum_{i=1}^{N} \vec{s}_i(u,v)\,.$$

Let $P(x, y, z)$ be the surface representation of a part in the 3D space obtained by:

$$P(x,y,z) = T(P(u,v))\,. \tag{18}$$

If we divide the 3D space, into boxes or voxels (volume elements), each point of the (x, y, z) coordinates will be contained in one of these voxels. Let $Inf(x)$ be the largest integer inferior or equal to x. For the point (x, y, z), it can be found that $x_i = Inf(x)$, $y_j = Inf(y)$, and $z_k = Inf(z)$. Thus the point (x, y, z) will be contained in the voxel V_{ijk} defined by the coordinates (x_i, y_j, z_k) and (x_i+1, y_j+1, z_k+1) (Fig. 9). If we extend the concept of a 2D binary bitmap, where each pixel (r, s) can take just one of two values, each voxel (i, j, k) in the 3D space can take one of two values: 0 (unoccupied) or 1 (occupied). An occupied voxel contains some portion of any of the surfaces that make up the part (Fig. 9).

Let us divide each surface $s_i(u, v)$ into $N_{u_i} \times N_{v_i}$ parts, with N_{u_i} and N_{v_i} as two thresholds that guarantee that when a surface is crossed by the 3D grid, more than one voxel will be touched in the 3D space. Thus, when we move over a surface, following its parametric coordinates, by steps of $\Delta u_i = \frac{u_{i1}-u_{i0}}{Nu_i}$ and $\Delta v_i = \frac{v_{i1}-v_{i0}}{Nv_i}$, it is possible to find all voxels in the 3D space that this surface touches (occupied voxels). The union of all the occupied voxels generated by the 3D

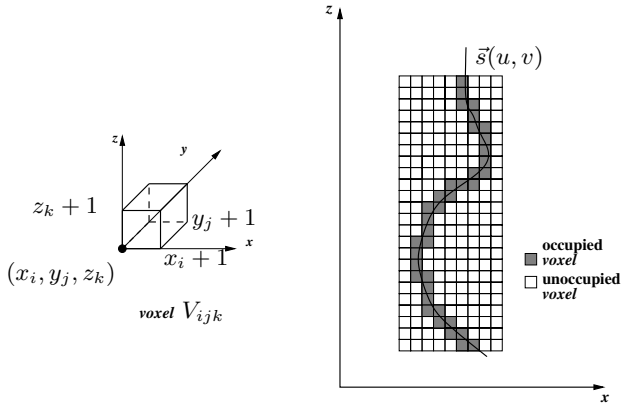

Fig. 9. The *voxel* V_{ijk} and the *voxel representation* of the profile of the surface $\vec{s}(u, v)$

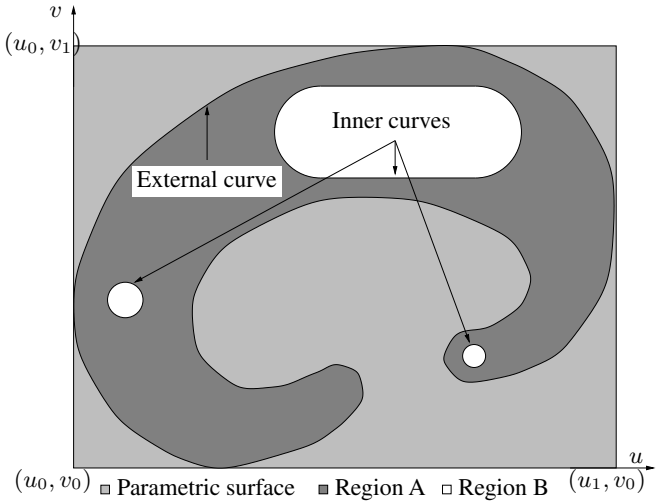

Fig. 10. Domain of variation for parameters u and v

surface representation of a part $P(u, v)$ is the *3D voxel model* of the part $P_D(x, y, z)$. Clearly, $P(x, y, z) \subseteq P_D(x, y, z)$. The importance of this *3D voxel model* in the solution of the occlusion problem will be detailed later.

5.2.2 Step 2: Find the viewpoint set

We now describe how the algorithm finds the set X of viewpoints for the acquisition system composed for the ASR sensor fixed to a CMM. The strategy could easily be adapted to other systems (range sensor plus mechanical support). In [12], we show how the strategy works for a system composed of a BIRIS range sensor (based on defocusing of the return beam) fixed on a robot arm.

The search for the set of viewpoints is conducted independently for each surface of interest and in three processes. It was shown in Sect. 5.1 that the optimal placement of the range sensor in order to acquire accurate 3D data is obtained when the laser beam (with $\gamma = 0°$) reaches the surface in the normal direction ($\alpha = 0°$ and $\beta = 0°$). The point (x_s, y_s, z_s) (Fig. 8) fulfills these conditions. In general, this will be the case when there are no occlusion or accessibility problems.

In the first step, a 2D binary representation of the surface is created (from the NURBS surface) and processed to obtain the viewpoint projection on the surface. Then the set of projected viewpoints is used to obtain the best viewpoint position in space by defining all its parameters (Step 2.2). Finally, if necessary, the viewpoint is modified to ensure the visibility of the surface to be digitalized (Step 2.3).

Step 2.1: Viewpoints projection on the surface. We define a viewpoint projection on the surface as the point where the laser beam reaches the surface when the sweep angle γ is equal to zero. We henceforth call this point the projected viewpoint. Initially we create a 2D representation of each surface. This image is processed to obtain the set of projected viewpoints. We denote as PVP_{s_i} the set of projected viewpoints on the surface $\vec{s}_i$.

Two-dimensional discrete and binary surface representation. Let $\vec{s}(u, v)$ be the equation of a parametric surface obtained from the CAD model. The variation range D for parameters u and v is defined by $D = \{(u, v) | u_0 \leq u \leq u_1, v_0 \leq v \leq v_1$ and, $(u, v) \in A \cap B\}$, with A being the inner component of the external curve and B the union of the external components of inner curves (Fig. 10).

We define the grid M on parametric space (u, v) with a sampling step Δ_{uv} such that:

$$\begin{aligned} &\|\vec{s}(u_i, v_j) - \vec{s}(u_i + \Delta_{uv}, v_j)\| \\ &\qquad = \|\vec{s}(u_i, v_j) - \vec{s}(u_i, v_j + \Delta_{uv})\| = 1 \end{aligned} \tag{19}$$

where $\|\vec{p_1} - \vec{p_2}\|$ represents the euclidean distance in R^3 between the points $\vec{p_1}$ and $\vec{p_2}$. For the grid M we define the discrete space (u^d, v^d) such that $u^d = 0, 1, 2..., q$ and $v^d = 0, 1, 2..., r$, with $q = Int(\frac{u_1 - u_0}{\Delta_{uv}} + 1)$ and $r = Int(\frac{v_1 - v_0}{\Delta_{uv}} + 1)$ and $Int(a)$ the integer part of a.

The 2D binary and discrete representation $\vec{s}_{db}(u^d, v^d)$ for the surface $\vec{s}$ is defined by:

$$\vec{s}_{db}(u^d, v^d) = \begin{cases} 1 \text{ if } (u^d, v^d) \in A \cap B \\ 0 \text{ otherwise} \end{cases} \tag{20}$$

In other words, $\vec{s}_{db}$ is equal to the set of points (u^d, v^d) from the grid included in $\vec{s}$.

The principal disadvantage of this type of discretization, known as discretization by inclusion, is that a very thin surface that does not contain any complete element of the grid M results in an empty discretization. This disadvantage is more obvious when we discretize a curved line, but this is not the case here because we are always working with surfaces. For thin surfaces, this disadvantage is overcome by defining a smaller sampling step in order to always have at least ten points (u^d, v^d) from the grid included in the surface.

Set of projected viewpoints. The 2D representation ($\vec{s}_{db}(u^d, v^d)$) of each surface is processed to obtain the set of projected viewpoints of the surface ($PVP_{s_i} \in \vec{s}_{db}(u^d, v^d)$). The process we chose is based on the concept of a skeleton. The skeleton is a representation that is centered and representative

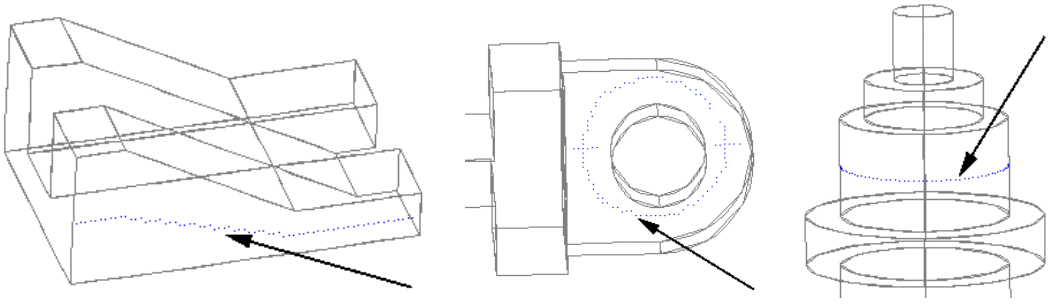

(a) Set on a flat surface (b) Set on a flat surface (c) Set on a curved surface

Fig. 11. Set of projected viewpoints involving flat and curved surfaces

of the shape of the object. Some properties of the skeleton are: it is simple (i.e., is made of arcs and curves), it comprises the same number of related components and holes as for the object, and it has the same shape as the object. These properties are very interesting for digitalization because the fact of being thin and connected makes it possible to be followed by the CMM by small movements; in addition, because it has the same form as the surface, we are able to digitalize the whole surface.

In Fig. 11, we illustrate the set of projected viewpoints found for two plane surfaces and for a curved surface (in the figure the set is highlighted by an arrow).

The orientation of the sweeping of the laser beam (parameter θ of the viewpoint) must be perpendicular to the direction of the sensor movement between the projected viewpoints in order to have a minimal distance between these points and the surface edges. By following the parametric directions of the surface $\vec{s}_{db}$, we determine the best sweeping direction of the laser beam as that where the variation of the incidence angle, during a complete sweeping from one edge of the surface to the other, is the smallest. The skeleton (set of projected viewpoints) is always constrained to have its propagation direction perpendicular to the best sweeping direction of the laser beam.

A CMM moves between two viewpoints in space following the line that connects the viewpoints. The sweeping of the laser beam is perpendicular to this line. The orientation of the range sensor during this movement remains constant. If the speed of this movement is smaller than the sweeping rate of the laser beam (usually it is), then the portion of the surface digitalized between the two points is defined by the rectangle $R = a \cdot b$, as shown in Fig. 12. Parameters a and b are a function of the distance d from the range sensor to the part, of the sensor field of view ($2 \times \gamma$ maximum, $2\gamma_{max}$), and of the distance between the two projected viewpoints. In most cases, the sensor field of view is fixed, for the ASR sensor it is $15°$ ($\gamma_{max} = \pm 7.5°$). The distance d is a parameter computed by the acquisition strategy according to the noise model of the sensor and is forced to remain between 170 mm and 240 mm (see Sect. 3). For our system, a is the line formed by the projection of the laser beam on the surface and is equal to $a \simeq 2d \cdot tan(\gamma_{max})$, and b is the distance between the two projected viewpoints (Fig. 12). The accuracy of the measured points by an ASR

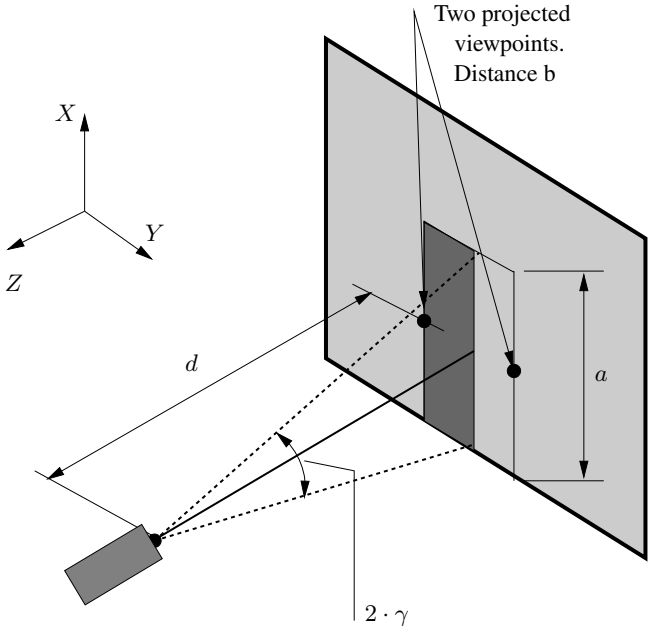

Fig. 12. Rectangle that defines the region digitalized between two viewpoints

sensor is a function of the distance d between the camera and the part, and of the incident angle of the laser beam on the surface, and is therefore related directly to parameters a and b.

We note in Fig. 11 that the distance from each projected viewpoint to the edges (sweeping distance) is symmetrical and as small as possible when measured perpendicularly to the direction of propagation of the projected viewpoints. The choice of a different orientation to measure the sweeping distance produces a larger sweeping distance, and for the viewpoint that means: *i.* The laser beam sweeps the surface with a major angle γ (i.e., a more significant angle of incidence) or *ii.* The ASR sensor is placed further from the surface. In both cases, the conditions of digitalization change and therefore so does the accuracy of the 3D data.

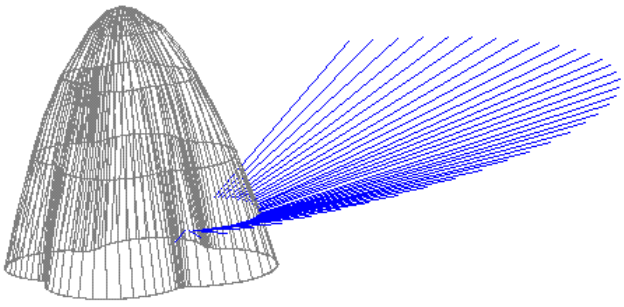

Fig. 13. Viewpoint set to digitalize a surface using the acquisition system

Step 2.2: Find the best viewpoint placement. In Step 2.1, we found the set of projected viewpoints of the surface (PVP_{s_i}). We know from Sect. 3 that the accuracy of the 3D data depends on parameters α, β, and d. We also know from Sect. 4 that a viewpoint is defined by seven parameters: $(x, y, z, \theta, \phi, \psi, \gamma)$. Now we will analyze how the viewpoint parameters are related to the parameters that control the accuracy of the 3D data, in order to define the best viewpoint placement to acquire accurate 3D data.

Let $P_{s_i} = (x_{P_{s_i}}, y_{P_{s_i}}, z_{P_{s_i}})$ be a projected viewpoint. Let P be a viewpoint related to the projected viewpoint P_{s_i}. The parameters for viewpoint P are:

- *Parameter* γ defines the amplitude of the sweeping of the laser beam. It does not affect the position of viewpoint. It must be considered only when an occlusion problem occurs (Step 2.3). The laser beam coming from viewpoint P reaches the projected viewpoint P_{s_i} when $\gamma = 0°$.
- *Parameter* θ defines the orientation of the sweeping of the laser beam when the mechanical support is moving the ASR sensor from one viewpoint to the next. It does not affect the position of a viewpoint.
- *Parameters* ϕ *and* ψ are the incident angle in the y and x direction, respectively, between the laser beam when it reaches the projected viewpoint on the surface and the normal vector to this point.
- *Position parameters* (x, y, z) are defined based on the ϕ and ψ parameters:

$$\begin{aligned} x &= x_{P_{s_i}} + d \cdot sin(\phi) \\ y &= y_{P_{s_i}} + d \cdot cos(\phi) \cdot sin(\psi) \\ z &= z_{P_{s_i}} + d \cdot cos(\phi) \cdot cos(\psi) \end{aligned} \tag{21}$$

A mapping from spherical to Cartesian coordinates is performed according to the direction of the laser beam and the distance d from the ASR sensor to the projected viewpoint P_{s_i}.

When the laser beam reaches the projected viewpoint P_{s_i} ($\gamma = 0°$) with an angle ϕ equal to α and an angle ψ equal to β (Fig. 2), the parameters of viewpoint P related to the projected viewpoint P_{s_i}, based on parameters α, β, and d that define the accuracy of the 3D data, are defined by:

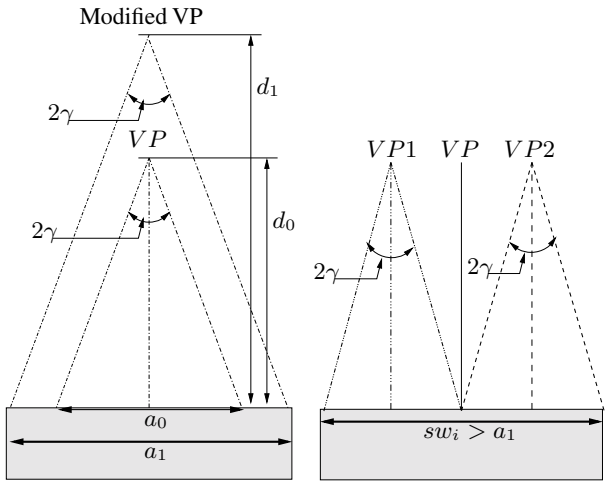

(a) Modification of d parameter

(b) New viewpoints by changing the position

Fig. 14. Digitalization of the whole width of the surface

$$\begin{aligned} \gamma &= 0° \\ \theta &= in\ the\ range\ [-90°, 90°] \\ \phi &= \alpha \\ \psi &= \beta \\ x &= x_{P_{s_i}} + d \cdot sin(\alpha) \\ y &= y_{P_{s_i}} + d \cdot cos(\alpha) \cdot sin(\beta) \\ z &= z_{P_{s_i}} + d \cdot cos(\alpha) \cdot cos(\beta) \end{aligned} \tag{22}$$

To compute parameters ϕ and ψ, we need the normal vector to the surface $\vec{s}_i$ at the projected viewpoint P_{s_i}. So we determine for P_{s_i} its equivalent point $(u, v) \in \vec{s}_i$ (by using Eq. 18), and we use the parameters of the NURBS surface. There is always a point (u, v) equivalent to the point P_{s_i} because $P_{s_i} \in PVP_{s_i} \in \vec{s}_{db}(u^d, v^d) \in \vec{s}(u, v)$. The normal vector to the point (u, v) is computed:

$$\overrightarrow{n} = \frac{\frac{\partial}{\partial u}\vec{s}(u,v) \times \frac{\partial}{\partial v}\vec{s}(u,v)}{\| \frac{\partial}{\partial u}\vec{s}(u,v) \times \frac{\partial}{\partial v}\vec{s}(u,v) \|^2} \tag{23}$$

with
$\frac{\partial}{\partial u}\vec{s}(u,v) = \frac{AB-CD}{B^2}$ and $\frac{\partial}{\partial v}\vec{s}(u,v) = \frac{EB-FD}{B^2}$ where

$A = \sum_{i=0}^{n}\sum_{j=0}^{m}(\frac{\partial}{\partial u}N_{i,p}(u))N_{j,q}(v)w_{i,j}\vec{P}_{i,j}$

$B = \sum_{i=0}^{n}\sum_{j=0}^{m}N_{i,p}(u)N_{j,q}(v)w_{i,j}$

$C = \sum_{i=0}^{n}\sum_{j=0}^{m}N_{i,p}(u)N_{j,q}(v)w_{i,j}\vec{P}_{i,j}$

$D = \sum_{i=0}^{n}\sum_{j=0}^{m}(\frac{\partial}{\partial u}N_{i,p}(u))N_{j,q}(v)w_{i,j}$

$E = \sum_{i=0}^{n}\sum_{j=0}^{m}N_{i,p}(u)(\frac{\partial}{\partial v}N_{j,q}(v))w_{i,j}\vec{P}_{i,j}$

$F = \sum_{i=0}^{n}\sum_{j=0}^{m}N_{i,p}(u)(\frac{\partial}{\partial v}N_{j,q}(v))w_{i,j}$

$\frac{\partial}{\partial u}N_{i,p}(u) = \frac{p}{u_{i+p-1}-u_{i-1}}N_{i,p-1}(u) - \frac{p}{u_{i+p}-u_i}N_{i+1,p-1}(u)$ and

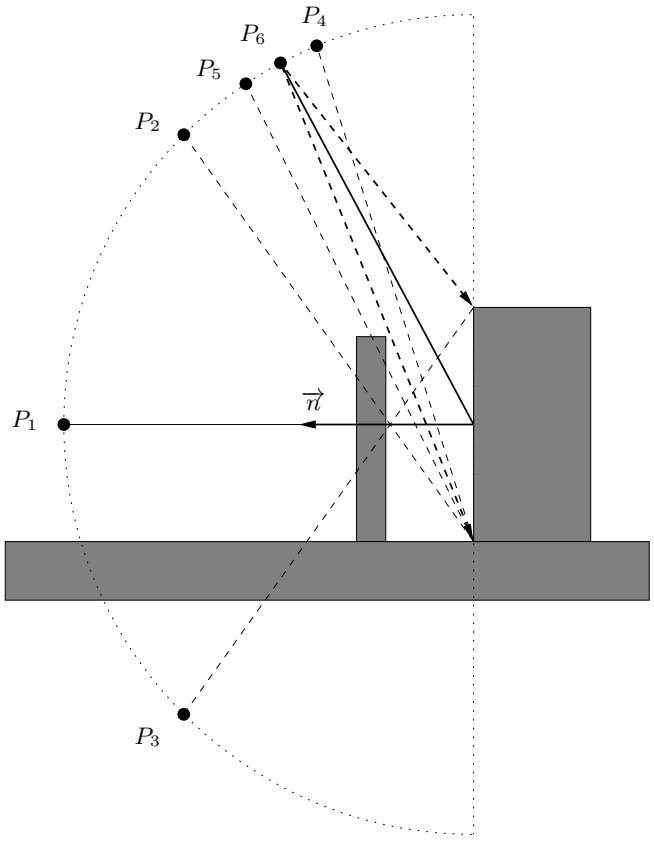

Fig. 15. Searching a new viewpoint without occlusion problems by changing its α or β parameter

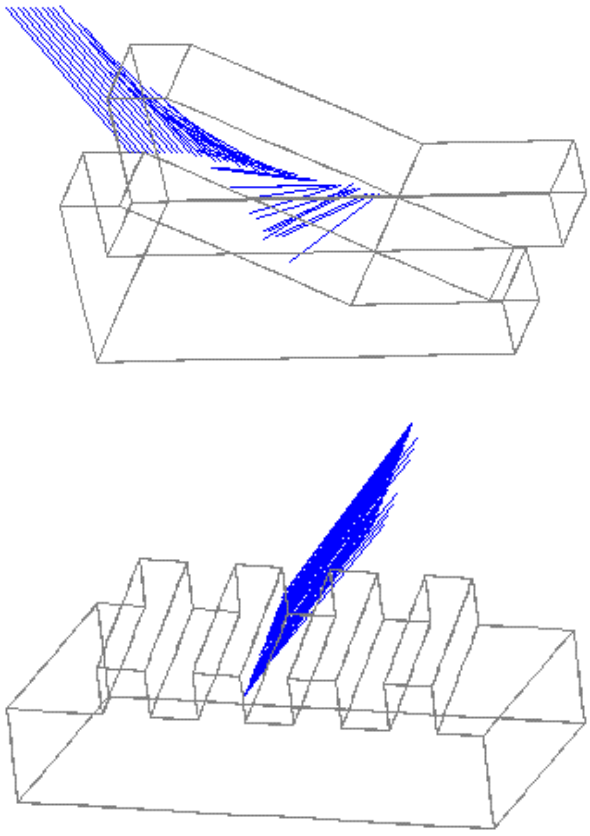

Fig. 16. New viewpoints to solve occlusion problems remaining as near as possible to the normal direction

$$\frac{\partial}{\partial v}N_{j,q}(v) = \frac{q}{u_{j+q-1}-u_{j-1}}N_{j,q-1}(v) - \frac{q}{u_{j+q}-u_j}N_{j+1,q-1}(v)$$

all the parameters for the above relations were defined for Eq. 17.

We can now compute the 3D space viewpoint placement. It is known from Sect. 5.1 that the accuracy of the 3D data will be best when the values of viewpoints α, β, and d are $0°, 0°$, and 195 mm, respectively. Thus if there are no occlusion problems, the viewpoint will be defined by $(\gamma, \theta, \phi = 0°, \psi = 0°, x = x_{P_{s_i}}, y = y_{P_{s_i}}, z = z_{P_{s_i}} + d)$ following the normal direction to the projected viewpoint. For each point belonging to the set of projected viewpoints PVP_{S_i} in the discrete space $s_{db}(u^d, v^d)$, we place the viewpoints within the optimum distance and orientation conditions. In Step 2.3, we will explain how the parameters α, β, and d are relaxed when there are occlusion problems.

In Fig. 13, we illustrate the viewpoints found to digitalize a small region of a curved part (corresponding to one surface in the CAD model). Each line represents the projection of the laser beam from the viewpoint where the sensor is placed in relation to the projected viewpoint when the sweeping angle (γ) is equal to zero. The free end of the line (in the space) represents parameters (x, y, z). The point where the line reaches the surface represents a projected viewpoint. The parameters α and β are equal to zero, so the propagation of the laser beam follows the normal direction for each projected viewpoint. The d parameter is the euclidean distance from the viewpoint to the projected viewpoint, that is, the line length.

Case when not all of the surface is covered. The width of surface $sw(P_{s_i})$ for a skeleton point is obtained by adding the distances from the point to each edge of the surface. Let $sw(P_{s_i})$ be the minimal distance that must be swept by the laser beam (passing by the point P_{s_i}) in order to digitalize the whole width of the surface. The optimal value of a (parameter of the digitalization rectangle), called a_0, is obtained when the viewpoint is placed under the optimal accuracy conditions ($\alpha = 0°, \beta = 0°$, and $d = 195$ mm) with respect to the projected viewpoint (P_{s_i}) and with $\gamma_{max} = \pm 7.5°$, so $a_0 = 51$ mm (Fig. 14). For point P_{s_i}, two cases can arise: $sw_i \leq a_0$ or $sw_i > a_0$. In the first case, except for occlusion problems, the viewpoint remains defined under the optimal accuracy conditions. For the second case, we must modify the parameters of the viewpoint.

We have two types of parameter modification required to widen a. The first consists of modifying parameter d up to its maximum value; therefore, $d = 240$ mm. For this value we define $a_1 = 63$ mm [Fig. 14(a)]. We modify d in order not to increase the number of viewpoints, even if we lose some accuracy of the 3D data. The other modification consists in defining new projected viewpoints. If $sw_i > a_1$, new projected viewpoints are defined and placed on the same line of the laser beam sweeping, at an equal distance between the point and the edge of the surface [Fig. 14(b)]. These two processes are repeated until the whole width of the surface is digitalized.

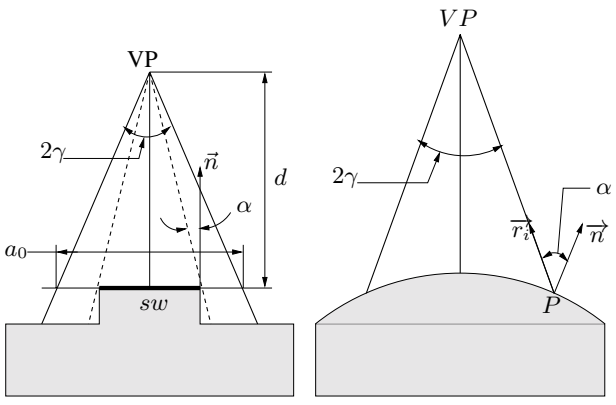

(a) For a field of view greater than the surface

(b) Estimation on a curved surface

Fig. 17. Evaluation of α and β parameters

Step 2.3: Verify the nonocclusion conditions. Until now, the viewpoints were found for the best accuracy conditions, i.e., placed at the optimal distance and with the optimal orientation. The following step of the strategy is to check if the viewpoint is free of occlusion problems, i.e., the laser beam is not intercepted by any object and can thus reach the desired surface. For the evaluation of nonocclusion conditions, a ray is traced from the viewpoint toward the area to digitalize. The strategy verifies (using the model voxel of the part $P_D(x, y, z)$) that no portion of the part is intersected by the ray, i.e., that the ray arrives freely to its objective.

When an occlusion problem is detected, the system searches a new viewpoint by changing its parameters α or β. The parameter d is not changed because, in general, it does not solve occlusion problems. The movement is performed by increasing or decreasing the incidence angle of the laser beam in the direction of the sweeping laser beam for parameter α, or perpendicular to it for parameter β. This process is illustrated in Fig. 15. The initial point P_1 defined under the best conditions of accuracy presents an occlusion problem. Points P_2 and P_3 do not solve the occlusion problem. P_4 provides a solution, but the strategy continues to seek a point that is closest to P_1 and finds P_5 and P_6. The process stops when the variation of the angle between two valid points is smaller than $5°$.

To obtain a new viewpoint, Eq. 16 is used, but we change the constraints imposed on α and β to be between the new values found (α_{fo}, β_{fo}) and the maximum value, so: $\alpha_{fo} \leq \alpha \leq 35°$ and $\beta_{fo} \leq \beta \leq 15°$. The solution of Eq. 16 allows us to define a viewpoint placement that is able to digitalize the desired area having good conditions relative to the accuracy of the 3D data. Sometimes α_{fo} and β_{fo}, the parameter values found, are such that $\alpha_{fo} > 35°$ and $\beta_{fo} > 15°$. In this case, there is no solution to the occlusion problem.

Figure 16 shows the new viewpoints found to solve the occlusion problems. We notice that the new viewpoints remain as close as possible to the normal direction. In the figure, each line represents the projection of the laser beam from the point where the sensor is placed (the free end) to the projected viewpoint on the surface.

Viewpoint accessibility. By accessibility we mean that the viewpoint must be reachable by the mechanical support. For accessibility, we must guarantee that the part is in the workspace of the system (ASR sensor/mechanical support). This space defines the area where the sensor could be moved. As stated in Sect. 3.1, for the acquisition system used, this space has the form of a parallelepiped with: $ws_x = 80\,\text{cm}$, $ws_y = 30\,\text{cm}$, and $ws_z = 30\,\text{cm}$. The viewpoint is transformed from the coordinate system of the part to the coordinate system of the workspace, and if we obtain a valid position, we say that the viewpoint is accessible.

In a valid position, the viewpoint is not superimposed on the part model. The strategy verifies that the viewpoint is not included within the voxel model of the part. All the parts used for this work are included in a volume of $100 \times 50 \times 50\,\text{mm}$ (Sect. 4.1). Since the placement distance of the viewpoint relative to the surface is usually at least $195\,\text{mm}$, we conclude that in general there are no accessibility problems. For parts with different sizes, an algorithm to detect the accessibility conditions using a complete model system (range sensor plus mechanical support) could be developed.

5.2.3 Step 3: Estimate 3D data accuracy

Once all the viewpoints have been located satisfying nonocclusion conditions, the strategy computes the accuracy of the 3D measured points from the obtained set of viewpoints. We know from Sect. 3 that the accuracy of the measured points by a range sensor is a function of the distance d between the camera and the part being digitalized and of the incident angles α and β of the laser beam. Thus, to estimate the accuracy of measured points, we must compute these parameters to each 3D acquired point. Here the angle α is dependent upon the instantaneous sweeping angle γ. Figure 17 illustrates some special configurations for the determination of α and β parameters. The parameter d was defined above.

Figure 17(a) illustrates the case where the field of view of the range sensor is greater than the width of the surface to measure. The angular amplitude of the sweeping ray is computed from the field of view $2 \cdot \gamma$ and distance d. The width of the surface sw is obtained from the CAD model.

In Fig. 17(b), we present the computation of the incident angle α over a curved surface. The point P where the ray touches the surface is computed by using the 3D surface model. The normal to the surface at this point is obtained from the NURBS surface. Finally, the angle α is computed by developing the inner product of two vectors $\vec{r_i} \cdot \vec{n}$.

Once parameters d, α, and β are known, the accuracy is computed as the sum of the noise introduced by each 3D point by using Eq. 1. The dispersion introduced by each parameter is obtained from the models developed in Sect. 3. Sometimes the required precision could not be obtained, particularly for surfaces having an occlusion problem. For such surfaces, the range sensor must have a large inclination to be able to scan the surface. When this happens, the system will indicate the regions that could not be digitalized with the required accuracy.

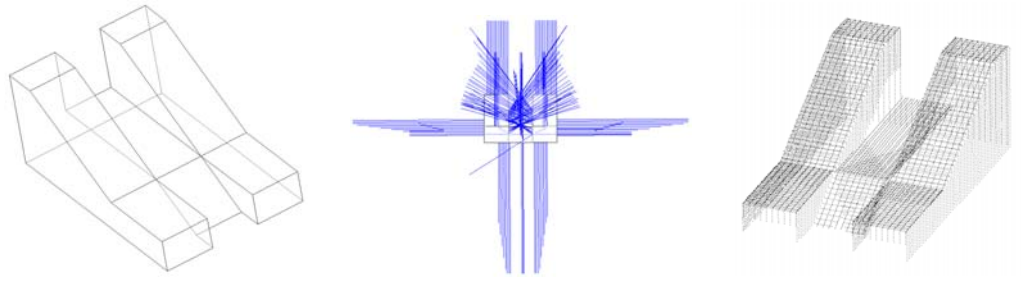

(a) Part 1, composed of flat surfaces

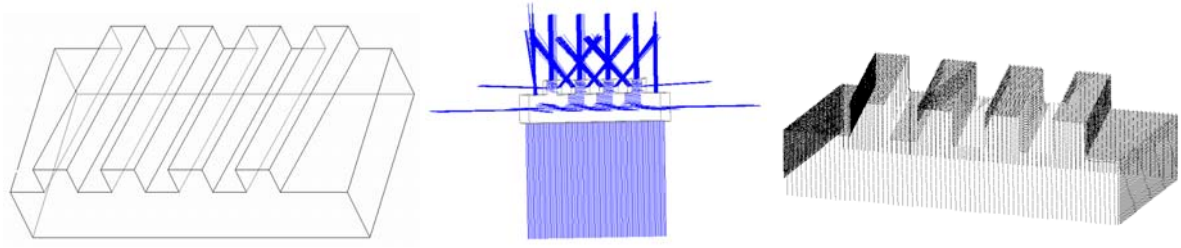

(b) Part 2, composed of flat surfaces

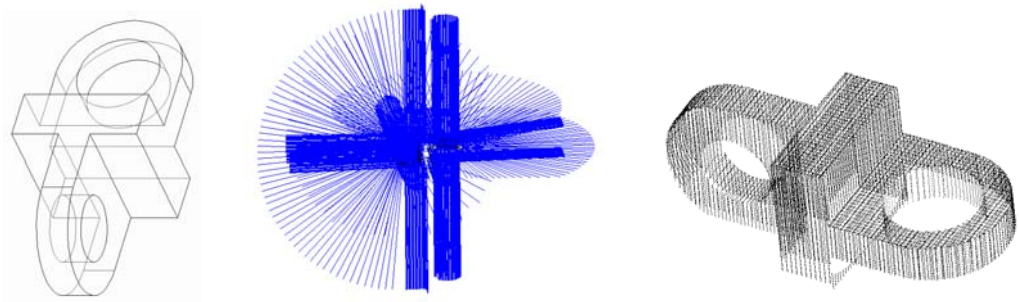

(c) Part 3, composed of flat and curved surfaces

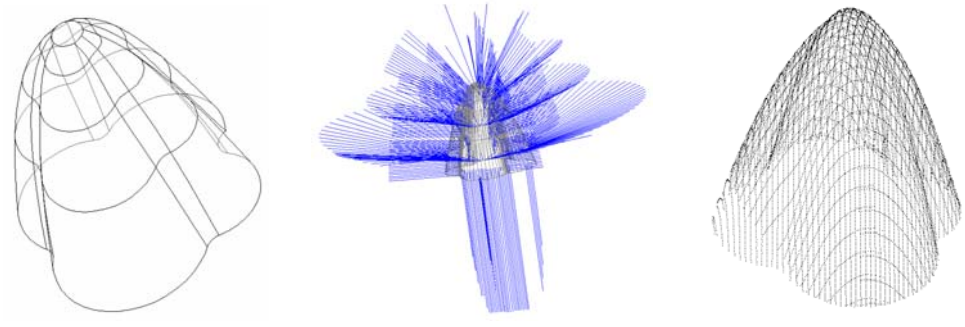

(d) Part 4, composed of curved surfaces

Fig. 18. CAD model, sensing strategy to digitalize and range images of some manufactured parts

5.2.4 Step 4: Distribute the set X of viewpoints

The last step of the strategy consists in distributing the set X of viewpoints in such a way that the parameters of two consecutive points are as similar as possible. The movement between the viewpoints is carried out by the mechanical support. It is desired that changes of the parameters from one viewpoint to another be minimal in order to reduce digitalization time.

For the acquisition system, because set X is derived from the skeleton of the surface, we have posed the problem as one of searching for the path of minimum cost in a graph. The problem is solved for each surface independently. The critical components of this method are: to have a good starting point, to know how the obtained results influence the choice of the next point, and to define a good criterion for stopping.

Let $P_{s_i i}$ be the i^{th} projected viewpoint of the set PVP_{s_i}, and let $V_8(P_{s_i i})$ be the number of points with 8-connectivity to $P_{s_i i}$. An extremal point is defined as having less connectivity with its neighbors and corresponds to the starting or stopping point of the digitalization path. We define as junction points those points with at least three 8-connectivity points.

The starting point is the extremal point closest to the origin of the surface in the parametric space. The (x, y, z) parameters of this point are compared with those of all the remaining points by computing the euclidean distance. The closest point is selected as the next point. If there are several points of equal distance, the distance between the (θ, ϕ, ψ) parameters is used. When a junction point is found, the selected path is that which minimizes the distance, and as soon as it arrives at an extremal point, the junction point is taken back to optimize the remaining junctions. This process is repeated until all points in PVP_{s_i} are taken into account. Since the set of projected viewpoints is finite (PVP_{s_i}), the set of viewpoints is also finite, and it is guaranteed that this process will terminate.

Free collision movement. The movement between two viewpoints must be collision-free. For this work we assume that within the workspace we only have the part. We have represented the part by a voxel model. The movement of the ASR sensor between two viewpoints is carried out by the mechanical support (CMM) following a straight line. The movement is accomplished without collisions when, after checking throughout this line, the model of the part is not touched. When a collision problem is detected, the system tries to solve it by defining intermediate positions of movement. For a more complex workspace (parts with different sizes, other parts in the workspace, etc.), an algorithm that takes into account the model of all the parts and the model of the acquisition system could be developed.

6 Sensor placement strategy results

In the previous section, we described our strategy to automatically set a sensor's placement for completely and accurately acquiring the geometry of a surface or of the complete part whenever possible. In this section, we present some results of a sensing strategy for the complete digitalization of some manufactured parts.

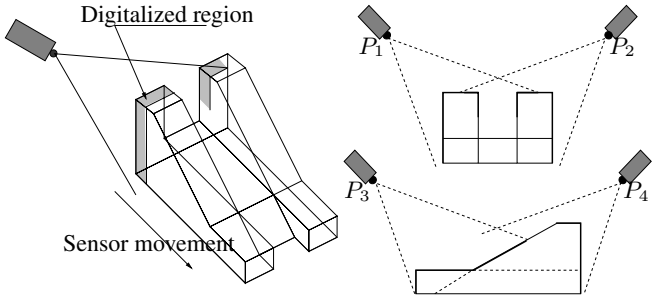

Fig. 19. Standard digitalization process

In Fig. 18, we show the CAD model, the sensing strategy for digitalization, and the range images of different manufactured parts, respectively. Part 1 [Fig. 18(a)] and part 2 [Fig. 18(b)] are composed of flat surfaces, part 3 [Fig. 18(c)] is composed of both flat and curved surfaces, and part 4 [Fig. 18(d)] is composed of curved surfaces.

The CAD model of each part is a wire model representing its NURBS surfaces. The sensing strategy is designed for the digitalization of the whole part and for an acquisition system composed of an ASR sensor mounted on a CMM. All the viewpoints are represented by a line that is the projection of the laser beam from the point where the sensor is placed (the free end) to the projected viewpoint on the surface. For inner surfaces, some occlusion problems were solved. The viewpoints always remain close to the normal direction of surfaces. Finally, we present the range images of the parts acquired by the acquisition system using the sensing strategy.

A *standard digitalization* is a systematic discretization of the part. It is a process in which the part is swept by the laser beam when the sensor is moved from one preset viewpoint to another (the viewpoints are manually selected). These viewpoints are at a fixed orientation with respect to the part. In this work, we swept the part from four different positions of the sensor, as shown in Fig. 19. The slope of the sensor was $45°$, and the sensor movement was from viewpoints P_1, P_2, P_3, and P_4 to another viewpoint perpendicular to the sheet.

In order to evaluate the improvement of the accuracy of the 3D data when they were acquired using the sensing strategy, a standard digitalization of each part was done. An accuracy evaluation of the two images of each part was done by using an algorithm that computes the distance between each measured point and the nearest point on the NURBS surface. We summarize in Table 1 the results of measurement of the average distance between each point of the cloud and the closest point on the NURBS surface. The average distance for the standard digitalization is shown in the column *Stand Dig*. The average distance for the digitalization using the sensing strategy is present in the column *Strat Dig*. In the last column, we present the improvement obtained when the strategy is used.

The smallest average distance is obtained for parts 1 and 2, which is not surprising since these parts are composed of flat surfaces. For these two parts, we obtain an improvement of about 33%. For the curved part (part 4), we obtain an improvement of 35%, which is better because in the digitalization process the laser beam is closer to perpendicular when we use the strategy. Finally, for part 3, some occlusions permit no more than a 13% improvement.

Table 1. Average distance between each point of the cloud and the closest point on the NURBS surface

Part	Stand Dig	Strat Dig	Improvement
Part 1	73 µm	48 µm	25 µm(34%)
Part 2	99 µm	66 µm	33 µm(33%)
Part 3	106 µm	92 µm	14 µm(13%)
Part 4	153 µm	100 µm	53 µm(35%)

7 Conclusion

We have presented an automated acquisition planning strategy to improve the accuracy of a cloud of measured 3D points. The strategy computes a set of viewpoints in order to obtain a complete and accurate 3D image of the part or selected surfaces of the part. The viewpoints are constrained to have the best accuracy conditions in the scanning process. For the range sensor used, it was shown that accuracy of the 3D measured points is a function of the distance to the part and of the incident angle with which the laser beam reaches the surface.

The system does not have any limitation in the geometry of parts to be scanned, meaning that it works as well with flat or curved parts. Knowledge of the exact position and orientation of the part and its CAD model are the only system requirements. The strategy can be easily adapted to use other kinds of range sensors and mechanical supports. For these, a new model of the sensor accuracy must be found.

The planning strategy allows us to digitalize the whole part or the surfaces of interest with a specified accuracy. This property is important for inspection tasks, where we are largely interested in verifying the specification of a few surfaces, because we are able to have an accurate cloud of 3D measured points of the surface.

Although some elements of the algorithm can be expensive in computation time, like the generation of the *voxel model* or the solution to occlusion problems, all of the processes for digitalization planning are carried out offline.

Acknowledgements. The authors wish to thank the anonymous reviewers for their useful comments and criticisms that greatly enhanced the quality of the paper.

References

1. Abrams S, Allen P, Tarabanis K (1997) Computing camera viewpoints in an active robot work-cell. Department of Computer Science, Columbia University, New York
2. Besl PJ, McKay ND (1992) A method for registration of 3-D shapes. IEEE Trans Patt Analysis Mach Intell 14(2):239–256
3. Blais F, Rioux M, Beraldin JA (1988) Practical considerations for a design of a high precision 3-D laser scanner system. In: Proceedings of SPIE conference on optomechanical and electro-optical design of industrial systems, Bellingham, WA, June 1988, pp 225–246
4. Mason SO, Grun A (1995) Automatic sensor placement for accurate dimensional inspection. Comput Vis Image Understand 61(3):454–467
5. Maver J (1995) Collecting visual information using an active sensor system. Ph.D. dissertation, Department of Computer and Information Science, University of Ljubljana, Ljubljana, Slovenia
6. Moron V, Boulanger P, Masuda P, Redarce HT (1995) Automatic inspection of industrial parts using 3-D optical range sensor. In: Proc SPIE Videometrics IV 2598:315–325
7. Moron V (1996) Mise en correspondance de données 3D avec un modèle CAO: Application à l'inpection automatique. Ph.D. dissertation, Automatique Industrielle, Institut National des Sciences Appliquées de Lyon (INSA), France
8. Papadopoulos-Orfanos D (1997) Numérisation géométrique automatique à l'aide d'un capteur de présicion à profondeur de champ réduite. Ph.D. dissertation, Ecole Nationale Supérieure des Télécomunications de Paris (ENST)
9. Piegl L, Tiller W (1997) The NURBS book, 2nd edn. Springer, Berlin Heidelberg New York
10. Pito R (1997) Automated surface acquisition using range cameras. Ph.D. dissertation, Computer and Information Science, GRASP Laboratory, University of Pennsylvania, Philadelphia
11. Prieto F, Redarce HT, Lepage R, Boulanger P (1998) Visual system for fast and automated inspection of 3D parts. Int J CAD-CAM Comput Graph 13(4-5-6):211–227
12. Prieto F, Redarce HT, Lepage R, Boulanger P (1999) Range image accuracy improvement by acquisition planning. In: Proceedings of the 12th conference on vision interface (VI'99), Trois Rivières, Québec, Canada, 18–21 May 1999, pp 156–163
13. Rioux M (1984) Laser range finder based on synchronized scanners. Appl Opt 23(21):3837–3844
14. Tarabanis KA, Allen PK, Tsai RY (1995a) A survey of sensor planning in computer vision. IEEE Trans Robot Automat 11(1):86–104
15. Tarabanis KA, Tsai RY, Allen PK (1995b) The MVP sensor planning system for robotic vision tasks. IEEE Trans Robot Automat 11(1):72–85
16. Tarabanis KA, Tsai RY, Anil K (1996) Computing occlusion-free viewpoints. IEEE Trans Patt Analysis Mach Intell 18(3):279–292
17. Tarbox GH, Gottschlich SN (1995a) IVIS: An integrated volumetric inspection system. Comput Vis Image Understand 61(3):430–444
18. Tarbox GH, Gottschlich SN (1995b) Planning for complete sensor coverage in inspection. Comput Vis Image Understand 61(1): 84–111
19. Trucco E, Umasuthan M, Wallace AM, Roberto V (1997) Model-based planning of optimal sensor placements for inspection. IEEE Trans Robot Automat 13(2):182–194
20. Whaite P, Ferrie F (1997) Autonomous exploration: driven by uncertainty. IEEE Trans Patt Analysis Mach Intell 19(3):193–205
21. Zha H, Morooka K, Hasegawa T, Nagata T (1997) Active modeling of 3-D objects: planning on the next best pose (NBP) for acquiring range images. In: Proceedings of the international conference on recent advances in 3-D digital imaging and modeling, Ottawa, Canada, 12–15 May 1997, pp 68–75

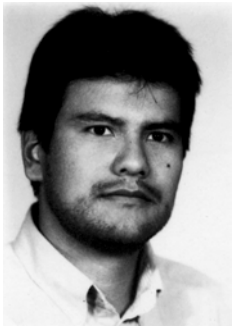

Flavio Prieto received a degree in electronic engineering in 1991 from Francisco José de Caldas Distrital University, a degree in physics in 1992 from the National University of Colombia, and his M.S. in electrical engineering in 1995 from Andes University, all in Bogotá, Colombia. He recived his Ph.D. in 2000 in industrial automation from the Institut National des Sciences Appliquées de Lyon, France and from the École de Technologie Supérieure, Université du Québec, Montréal, Canada. His Ph.D. dissertation was developed in cooperation between the two universities. Since February 2000 he has been working as an assistant professor in the Department of Electrical Engineering at the National University of Colombia at Manizales. His research interests include computer vision, image processing, automated inspection systems, and pattern recognition.

Richard Lepage received his B.S. in electrical engineering in 1974, his M.S. in signal processing in 1982, and his Ph.D. for work on applications of artificial neural networks to computer vision in 1994, all from Laval University, Québec, P.Q., Canada. He is currently a professor in the Department of Automated Production, École de Technologie Supérieure, Université du Québec, Montréal, P.Q. From 1976 to 1989, he was with the Defense Research Establishment, Valcartier, P.Q., Canada. His research interests include neural networks, computer vision, 3-D vision, automated inspection systems, and the use of artificial intelligence techniques in agrifood quality control.

Pierre Boulanger graduated from Laval University in engineering physics. He also received his M.S. in physics from the same university and his Ph.D. in electrical engineering from the University of Montreal. He worked for 18 years at the National Research Council of Canada as a senior research officer where his primary research interests were in 3-D computer vision, rapid product development, and virtualized reality systems. Since 1 July 2001, he has been working as a tenured associate professor in the Departm ent of Computing Science at the University of Alberta doing research on and teaching about virtualized reality systems. He has published more than 100 scientific papers in various journals and conferences. He is on the editorial board of two major academic journals and is the program chair of the 3DIM2003 conferences. Dr. Boulanger is also on many international committiees and frequently gives lectures on rapid product development and virtualized reality. He is the founder of the Canadian Virtualized Reality Systems Working Group. He is also the Director of the Advanced Man Machine Interface Laboratory. On the commercial side, Dr. Boulanger is the president of PROTEUS Consulting Inc., an Alberta-based consulting firm specializing in virtual reality applications.

Hervé T. Redarce received his Ph.D. and Habilitate Doctor in electrical engineering with a specialization in robotics and 3-D imaging from Institut National Polytechnique de Grenoble and Institut National des Sciences Appliquées de Lyon. He was an assistant professor for 15 years in the Department of Mechanical Engineering (INSA) and then professor in the Department of Electrical Engineering (INSA). In 1999, Dr. Redarce was a visiting researcher at the Laboratoire d'Imagerie de Vision et d'Intelligence Artificielle de l'Ecole de Technologie Supérieure de l'Université du Québec in Montréal (Canada). Since 2000 he has been the head of the laboratory's robotics research team. His interests include medical robotics, mechatronics systems, and robotics vision. He has authored more than 20 papers in international journals and 50 communications in international congresses.